Journal of Physics: Condensed Matter

Thermal expansion, polarization and phase diagrams of $Ba_{1-y}Bi_{2y/3}Ti_{1-x}Zr_xO_3$ and $Ba_{1-y}La_yTi_{1-y/4}O_3$ compounds

To cite this article: Michail Gorev *et al* 2009 *J. Phys.: Condens. Matter* **21** 075902

J. Phys.: Condens. Matter **21** (2009) 075902 (7pp) doi:10.1088/0953-8984/21/7/075902

Thermal expansion, polarization and phase diagrams of $Ba_{1-y}Bi_{2y/3}Ti_{1-x}Zr_xO_3$ and $Ba_{1-y}La_yTi_{1-y/4}O_3$ compounds

Michail Gorev[1,2], Vitaly Bondarev[1,2], Igor Flerov[1,2], Mario Maglione[3], Annie Simon[3], Philippe Sciau[4], Madona Boulos[5] and Sophie Guillemet-Fritsch[5]

[1] L V Kirensky Institute of Physics, Siberian Division, Russian Academy of Sciences, Akademgorodok, Krasnoyarsk, 660036, Russia
[2] Institute of Engineering Physics, Siberian Federal University, av. Svobodny 79, Krasnoyarsk, 660041, Russia
[3] ICMCB-CNRS, Universitè de Bordeaux I, 87 avenue A Schweitzer, 33608 Pessac, France
[4] CEMES-CNRS, Universitè de Toulouse, 29 rue Jeanne Marvig, 31055 Toulouse, France
[5] CIRIMAT CNRS/UPS/INPT, Universitè de Toulouse, Batiment 2R1, 118 route de Narbonne, 31062 Toulouse, France

E-mail: gorev@iph.krasn.ru, maglione@icmcb-bordeaux.cnrs.fr and sciau@cemes.fr

Received 20 November 2008, in final form 29 December 2008
Published 20 January 2009
Online at stacks.iop.org/JPhysCM/21/075902

Abstract
The thermal expansion properties of the ceramic compositions $Ba_{1-y}La_yTi_{1-y/4}O_3$ ($y = 0.0$, 0.026, 0.036, 0.054) and $Ba_{1-y}Bi_{2y/3}Ti_{1-x}Zr_xO_3$ ($y = 0.10$; $x = 0.0$, 0.04, 0.05, 0.10, 0.15) were determined in the temperature range 120–700 K. We report the temperature-dependent measurements of the strain, thermal expansion coefficient and the magnitude of root mean square polarization. The results obtained are discussed together with the data on the structure and dielectric properties.

1. Introduction

Barium titanate based solid solutions attract considerable interest owing to the rich diversity of their physical properties and various possible technological applications. Pure $BaTiO_3$ exhibits three ferroelectric phase transitions: cubic ($Pm3m$) → tetragonal ($P4mm$) → orthorhombic ($C2mm$) → rhombohedral ($R3m$) at $T_c \sim 401.8$ K, $T_1 \sim 299.5$ K and $T_2 \sim 210$ K, respectively. For many years A- and B-site dopants have been used to modify the electrical properties of $BaTiO_3$ based ceramics [1–6]. Many of these compounds are characterized by both ferroelectric and relaxor properties depending on the composition.

Isovalent dopants are commonly used to alter phase transition temperatures. Common nonferroelectric active B-site dopants such as Zr^{4+} and Sn^{4+} cause an almost linear decrease in T_c, whereas both T_1 and T_2 were found to be increased [6, 7]. The original ferroelectric transitions of $BaTiO_3$ are merged for $x \gtrsim 0.15$ into one cubic → rhombohedral transition. Further increase in the Zr concentration would result at $x \gtrsim 0.25$ in a ferroelectric relaxor behaviour similar to that of the canonical relaxors [7]. The relaxor features of $Ba(Ti_{1-x}Zr_x)O_3$ are connected with their compositional inhomogeneity or disorder and also with the presence of polar nanodomains in the nonpolar matrix. The nature and mechanism of the compositional disordering and the relaxor behaviour in Ba-containing compounds have been widely discussed [8–10]. The size of the Zr^{4+} ion (72 pm) is about 20% larger than that of the Ti^{4+} ion (60.5 pm) in 6 coordination, and random elastic fields are thus expected from this substitution, which are very likely to be responsible for relaxor properties which appear for $x \gtrsim 0.25$.

The heterovalent substitution of Ba^{2+} cations with the Bi^{3+} ones in $BaTi_{1-x}Zr_xO_3$ compounds can allow the addition of further disorder on the B-sites of the perovskite lattice. It has been suggested [11] that heterovalent substitutions could

induce a relaxor behaviour at low concentrations of Zr. The difference in valences of Ba and Bi would be, in that case, the more relevant parameter, and the corresponding random fields are thus expected to be electrical in nature.

The T_c value for $Ba_{1-y}Bi_{2y/3}TiO_3$ compounds is practically stable up to the value $y = 0.10$; however, the two dielectric permittivity anomalies at temperatures T_1 and T_2 merged for $y > 0.02$ into one at T'_m which arises within the ferroelectric state and is characterized by significant frequency dispersion [12]. Such a succession of phenomena is very unusual in the field of relaxors. Zr substitution in $Ba_{0.9}Bi_{0.067}(Ti_{1-x}Zr_x)O_3$ decreases T_c and increases T'_m up to a composition $x \approx 0.07$, beyond which there remains a single effect at T''_m with a strong dispersion, characteristic of relaxor behaviour [12].

The effect of the heterovalent substitution of Ba^{2+} cations with the La^{3+} ones on T_c, T_1 and T_2 is quite different. These values decrease very rapidly with increase in La concentration [13, 14]. The intermediate tetragonal–orthorhombic and orthorhombic–rhombohedral transition lines disappear for La concentrations greater than 5 at.% [13].

In this work we studied the thermal expansion of $Ba_{1-y}Bi_{2y/3}Ti_{1-x}Zr_xO_3$ and $Ba_{1-y}La_yTi_{1-y/4}O_3$ solid solutions with the aims of clarifying the phase diagrams and determining the polarization from thermal strain data. It is always a challenge to measure the temperature dependence of the polarization of ceramic materials. Thermal expansion, which is related to the square of the polarization, can be used to study phase transition, the thermal expansion coefficient and to estimate the magnitude of polarization in the ferroelectric and relaxor systems.

2. Experimental details

2.1. Bi^{3+} doped sample preparation and characterization

The compositions of the $Ba_{0.9}Bi_{0.067}(Ti_{1-x}Zr_x)O_3$ system were obtained from $BaCO_3$, Bi_2O_3, TiO_2 and ZrO_2 using the reaction [12]:

$$0.9BaCO_3 + 0.0335Bi_2O_3 + (1-x)TiO_2 + xZrO_2 \rightarrow Ba_{0.9}Bi_{0.067}(Ti_{1-x}Zr_x)O_3 + 0.9CO_2.$$

Before the two heat treatments, grinding was carried out for 1 h and powders were pressed under 100 MPa into 8 mm diameter discs about 5 mm thick. Calcination at 1200 °C for 15 h was followed by 4 h sintering at 1400 °C under an oxygen atmosphere.

Room temperature powder x-ray diffraction patterns were recorded on a Philips diffractometer using Cu Kα radiation ($\lambda = 0.154\,06$ nm) in the angular range $5° \leqslant 2\theta \leqslant 80°$. This made it possible to verify that the samples were single phase and of perovskite type. This allows us to determine the limits of the solid solutions. The single phase corresponds to $0 \leqslant x \leqslant 1$. The diameter shrinkage $(\Phi_{init} - \Phi_{final})/\Phi_{init}$ and the compactness (experimental density/theoretical density) were systematically determined. Their values were in the ranges 0.15–0.17 and 0.92–0.96, respectively.

Table 1. Structure, chemical composition and compactness (experimental density/theoretical density) of different doped barium titanate powders $Ba_{1-y}La_yTi_{1-y/4}O_3$.

y	Structure	Composition	Compactness
0.00	Tetragonal	$BaTiO_3$	0.955
0.026	Cubic	$Ba_{0.974}La_{0.026}Ti_{0.993}O_3$	0.900
0.036	Cubic	$Ba_{0.964}La_{0.036}Ti_{0.991}O_3$	0.907
0.054	Cubic	$Ba_{0.946}La_{0.054}Ti_{0.986}O_3$	0.921

2.2. La^{3+} doped sample preparation and characterization

The La-doped $BaTiO_3$ powder was synthesized by the oxalate method followed by a calcination treatment [15]. Samples of composition $Ba_{1-y}La_yTi_{1-y/4}O_3$ were prepared with different x values (0, 0.026, 0.036, 0.054). The starting materials were $BaCl_2{\cdot}2H_2O$, $TiCl_3$ and $LaCl_3{\cdot}7H_2O$. They were dissolved in water in various proportions and the co-precipitation was performed by addition of a solution of oxalic acid dissolved in ethanol. The solution was aged for a couple of hours, and the obtained precipitate was centrifuged. The precursors were then pyrolysed in air at 850 °C for 4 h to obtain the oxides. These powders were mixed with an organic binder, then uniaxially pressed into disks (diameter 6 mm and thickness 2 mm) under 250 MPa pressure.

The chemical composition of the oxide powder was determined accurately by induced coupled plasma spectroscopy (ICP AES Thermo-Optec ARL 3580). The structure was determined by x-ray diffraction analysis: a SEIFERT XRD-3003-TT diffractometer using Cu Kα radiation collected the data.

The chemical composition and the structure of the different powders prepared by pyrolysis of oxalate precursors at 850 °C for 4 h are reported in table 1. Undoped $BaTiO_3$ prepared by co-precipitation crystallizes in the tetragonal form whereas the cubic phase is observed when the powders are doped with La^{3+} ($y \geqslant 0.026$). The smaller La^{3+} cation stabilizes the cubic form as predicted by Goldschmidt's tolerance factor for undistorted and distorted perovskites [16].

2.3. Thermal expansion measurements

Thermal expansion measurements were performed in the temperature range 120–700 K with a heating rate of 5 K min^{-1} on the ceramic samples using a Netzsch model DIL-402C pushrod dilatometer with a fused silica sample holder. The results were calibrated by taking SiO_2 and Al_2O_3 as the standard reference, removing the influence of thermal expansion of the system.

2.4. Dielectric measurements

Dielectric measurements were performed on ceramic discs after deposition of gold electrodes on the circular faces by cathodic sputtering. The real and imaginary relative permittivities ε'_r and ε''_r were determined under helium as a function of both temperature (77–600 K) and frequency (10^2–2×10^5 Hz) using a Wayne–Kerr 6425 component analyser.

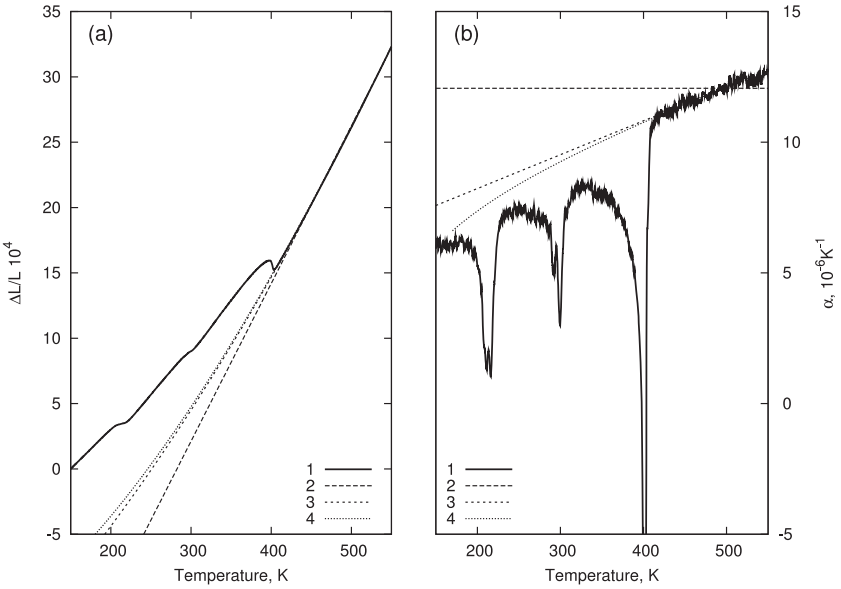

Figure 1. Thermal expansion $\Delta L/L$ (a) and thermal expansion coefficient α (b) as a function of temperature for $BaTiO_3$: experimental data (1) and approximation of lattice contributions by method A (2), method B (3) and method C (4).

3. Results and discussion

3.1. $BaTiO_3$

The thermal strain and thermal expansion coefficient as a function of temperature for pure $BaTiO_3$ are presented in figure 1. The linear thermal expansion coefficient $\alpha(T)$ shows three anomalies, connected with the phase transitions $Pm3m \rightarrow P4mm \rightarrow C2mm \rightarrow R3m$, at $T_c = 401.8$ K, $T_1 = 299.5$ K and $T_2 = 216.1$ K. The received values of thermal expansion coefficient agree well with the data [17, 18], especially in the region above the phase transition temperature between cubic and tetragonal phases.

Thermal expansion, which is related to the square of the polarization, can be used to study the polarization in the ferroelectric and relaxor systems. The value of root mean square polarization $\langle P^2\rangle^{1/2}$ can be extracted using the relation

$$\frac{\Delta L}{L} = \int \alpha_L(T)\,\mathrm{d}T + (Q_{11} + 2Q_{12})\langle P^2\rangle, \qquad (1)$$

where α_L is the lattice (regular) contribution to the thermal expansion coefficient and Q_{11}, Q_{12} are the electrostrictive coefficients.

Correct extraction of the anomalous contribution to the strain $(Q_{11} + 2Q_{12})\langle P^2\rangle$ related to the polarization is very important. We have tried to carry out this procedure by several methods. Electrostrictive constants Q_{11} and Q_{12} are determined in the paraelectric phase and considered to be constant [21, 22]. The results of polarization calculations are presented in figure 2. Here one can also see $P(T)$ data [19], deduced from ferroelectric $(P–E)$ hysteresis measurements in the tetragonal phase and the results of $P(T)$ estimation for 1100 nm $BaTiO_3$ film from the heat capacity [20].

Firstly, similar to previous approaches [23–25], we approximate $\Delta L/L(T)$ data at high temperatures $(T > T_c)$ by a straight line (method A). But this approximation is poorly defined, as we detect some deviations from the linear temperature dependence of strain and variation of the thermal expansion coefficient $\alpha(T)$ (figure 1). The temperature of nonzero anomalous strain contribution arising and the value of polarization calculated depend appreciably on the range in which the high temperature data are fitted.

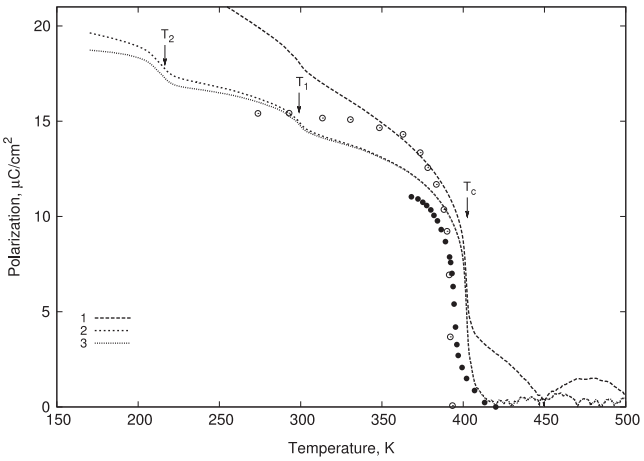

Figure 2. Polarization as a function of temperature for $BaTiO_3$ obtained by method A (1), method B (2) and method C (3): ○, data from [19]; ●, data from [20].

According to the Grüneisen theory, the expansion coefficient at high temperature (greater than Debye temperature Θ_D) is a slowly varying function of temperature. In addition, the contribution to strain may arise at high temperatures due to thermally generated defects. The increase of the imaginary part of the low-frequency permittivity at $T > 400$ K is related to increasing conductivity due to defect generation [12]. At high temperatures, $\alpha(T)$ shows a nearly linear temperature

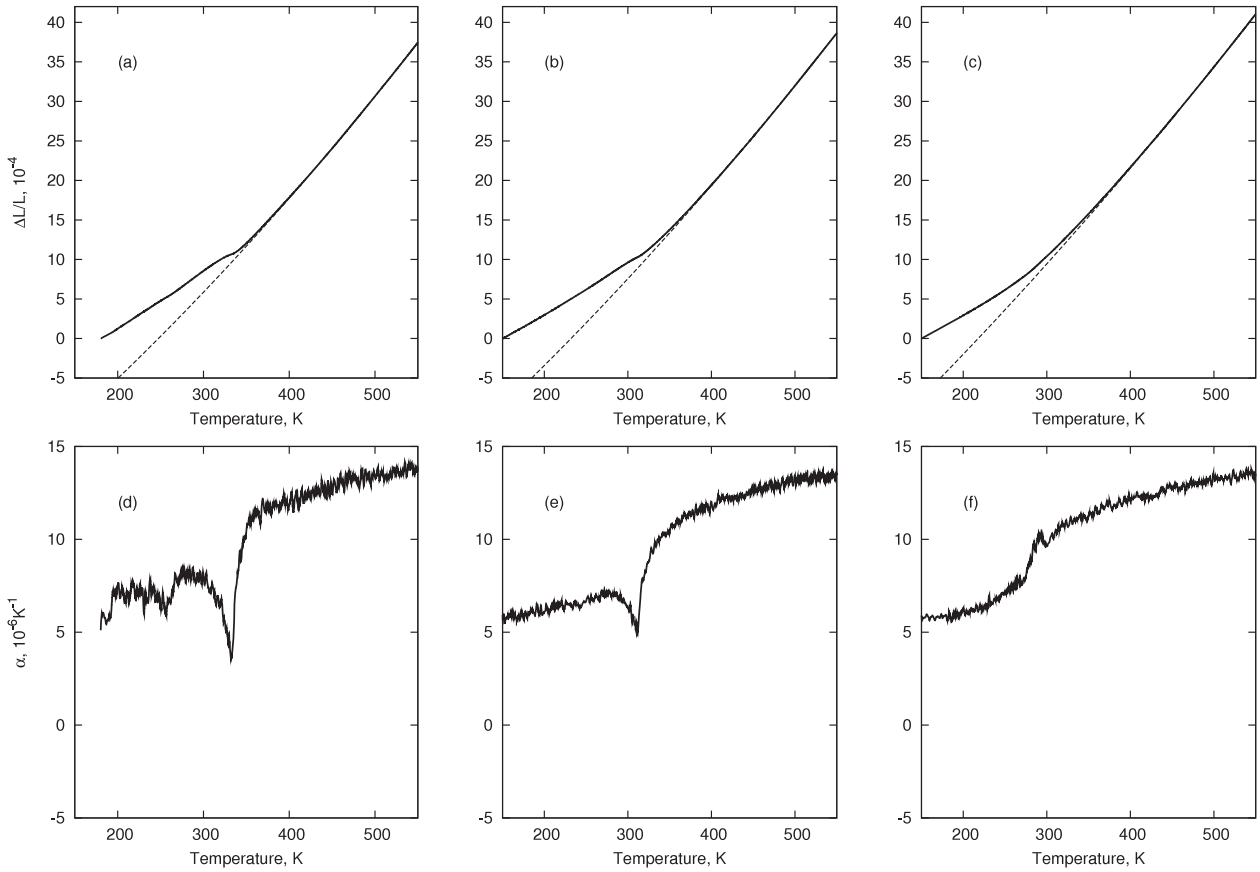

Figure 3. Temperature dependences of the dilatation $\Delta L/L$ and the thermal expansion coefficient α of $Ba_{1-y}La_yTi_{1-y/4}O_3$ compounds (——, experimental data; - - - -, high temperature approximation of lattice contribution by method C): (a), (d) $y = 0.026$; (b), (e) $y = 0.036$; (c), (f) $y = 0.054$.

dependence and we try to approximate the regular thermal expansion coefficient by equation $\alpha_L(T) = a + bT$ (method B). Accounting for these contributions considerably improves the approximation of the temperature dependence of $\alpha(T)$ and strain at $T > T_c$ (figure 1) and reduces the value of polarization in the low temperature region (figure 2). However, such an approach is not completely correct.

As the temperature is decreased the thermal expansion coefficient should tend to zero, and for a polarization estimation in the low temperature region ($T < T_c < \Theta_D$) it is necessary to consider the relation between thermal expansion and heat capacity and its temperature dependence, at least within the Debye model. As the thermal expansion coefficient in a cubic phase ($T > T_c \approx \Theta_D$) has only a weak dependence on the temperature, and it is almost impossible to define the Debye temperature from an approximation of experimental data, we use the average value of $\Theta_D \approx 432$ K [26]. The data were approximated by the relation (method C)

$$\alpha(T) = aT + bC_D(T), \tag{2}$$

where,

$$C_D(T) = 9R\left(\frac{\Theta_D}{T}\right)^3 \int_0^{\Theta_D/T} t^4 \frac{\exp(t)}{(\exp(t)-1)^2}\,dt. \tag{3}$$

Figure 2 shows the calculated temperature dependence of polarization. In our opinion the last method (method C) is more correct. That is the reason why we use it to extract the anomalous contribution to the strain and to obtain the root mean square polarization for all compounds studied.

3.2. $Ba_{1-y}La_yTi_{1-y/4}O_3$ compounds

3.2.1. Thermal expansion of $Ba_{1-y}La_yTi_{1-y/4}O_3$ solid solutions. The results of thermal expansion measurements of $Ba_{1-y}La_yTi_{1-y/4}O_3$ ceramics are represented in figure 3.

The anomaly of $\alpha(T)$ at T_c diminishes progressively as a result of increase in La concentration, but remains sufficiently sharp and is easily fixed for compounds with $y = 0.026$ and $y = 0.036$. The pre-transition phenomena above T_c become more noticeable. Anomalies at T_1 and T_2 decrease and smooth out much faster. Already at $y = 0.036$ they practically merge and turn to a shoulder on the low temperature site of the anomaly at T_c. Occurrence of the anomalous component in $\alpha(T)$ in a cubic phase is observed approximately at the same temperature 400–420 K for all compounds. The behaviour of thermal expansion coefficient $\alpha(T)$ correlates with the behaviour of dielectric permittivity $\varepsilon(T)$ [13, 14].

3.2.2. Phase diagram. The phase diagram of the system is presented in figure 4 where the data obtained from thermal expansion measurements as well as the results of studies of dielectric properties [13, 14] are shown. In the concentration

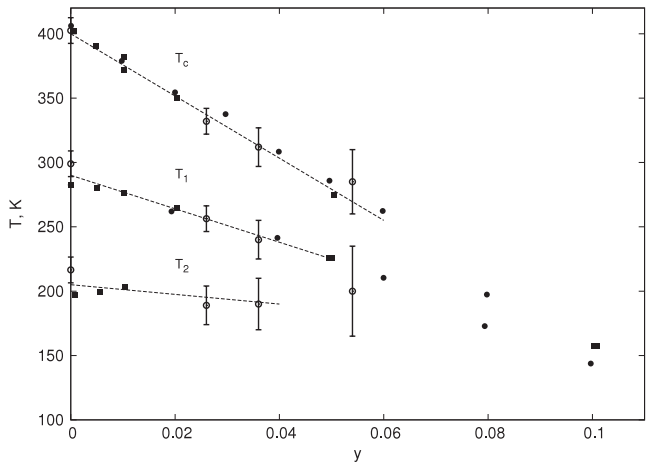

Figure 4. Variations of the transition temperatures T_c, T_1 and T_2 with composition for ceramics of the $Ba_{1-y}La_yTi_{1-y/4}O_3$ system.

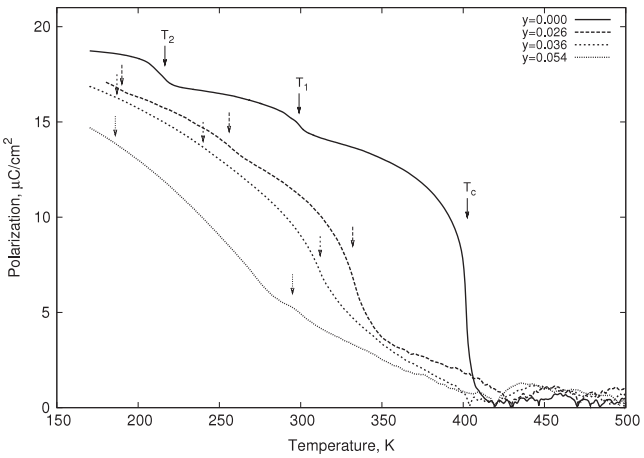

Figure 5. Root mean square polarization of $Ba_{1-y}La_yTi_{1-y/4}O_3$ compounds.

range studied the data for T_c and T_1 agree well. However, unlike [13] we have not found an obvious increase of T_2 with La concentration and disappearance of the C2mm phase.

The effect of La doping on the sequence of phase transitions in $BaTiO_3$ is explained by a combination of A- and B-site doping effects. In the case of La^{3+} doping charge compensation occurs via an ionic mechanism with partial replacement of Ba^{2+} by La^{3+} and the creation of titanium vacancies (the chemical formula $Ba_{1-y}La_yTi_{1-y/4}\square_{x/4}O_3$) leading to significant change in the ferroelectric active B-site [14]. The replacement of Ba^{2+} by the smaller La^{3+} cation on the A-site and the presence of B-site vacancies result in a rapid decrease in T_c. The Ti vacancies on the B-site disrupt the cooperative effects between octahedra in a similar manner to Zr^{4+} and Sn^{4+} doping [1, 2].

The increasing frequency dependence of ε below T_c with increasing y [14] is attributed to the increase in concentration of La^{3+} on the A-site and Ti vacancies on the B-site. La^{3+} ions and cation vacancies can form defect clusters and produce corresponding random electric fields. At high values of the La concentration long-range ferroelectric order can be broken down by defect clustering, but the local polar order is preserved within defect-free regions.

3.2.3. Root mean square polarization. Figure 5 shows the temperature dependence of the polarization calculated from the thermal strain data using equation (1). For solid solutions $Ba_{1-y}La_yTi_{1-y/4}O_3$ we used the same values of electrostriction coefficients as for $BaTiO_3$.

As La concentration increases, the polarization becomes more and more smoothed out and exists in a wide temperature range above T_c. The deviation of the strain from regular behaviour and the occurrence of nonzero polarization in solid solutions is observed at temperatures close to 420 K, considerably exceeding transition temperatures in the ferroelectric phase T_c. Such deviations are connected with the occurrence of polar nanoregions with random orientation of polarization in a paraelectric phase at temperatures lower than the so-called Burns temperature T_d [23], and are observed in some ferroelectric materials as well as in ferroelectric-relaxors in the study of various physical properties [24]. For solid solutions $BaTi_{1-x}Sn_xO_3$ the increase in the Burns temperature was revealed with increase in Sn concentration [17]. In our case the Burns temperature is almost constant; however, the temperature T_c decreases much faster than in $BaTi_{1-x}Sn_xO_3$ so that the difference $T_d - T_c$ changes linearly with La concentration from ∼10 K for $y = 0$ to ∼150 K for $y = 0.054$.

3.3. Thermal expansion of $Ba_{1-y}Bi_{2y/3}Ti_{1-x}Zr_xO_3$ compounds

The heat capacity $C_p(T)$ and the thermal expansion $\alpha(T)$ of two $Ba_{0.9}Bi_{0.067}(Ti_{1-x}Zr_x)O_3$ ($x = 0.04, 0.15$) ceramics were measured earlier [10] using an adiabatic calorimeter and an opto-mechanical dilatometer in the temperature range 100–420 K. Both compounds reveal diffuse heat capacity and thermal expansion anomalies: three anomalies in the temperature regions 150–250 K, 250–300 K and 300–400 K at $x = 0.04$ and two anomalies in the regions 200–250 K and 250–350 K at $x = 0.15$. Here we studied the thermal expansion of solid solutions with the same and other ($x = 0.0$, 0.05 and 0.10) compositions in wide temperature range to extract anomalous contributions, to obtain the root mean square polarization more correctly and to confirm the existence of additional thermal expansion anomalies at temperatures between T_c and T_m' for compounds with $x < 0.07$ [10].

The results of permittivity and thermal expansion studies on $Ba_{0.9}Bi_{0.067}Ti_{1-x}Zr_xO_3$ compounds are presented in figure 6. The T–x phase diagram of system (figure 7) is constructed using both the results of the present dielectric permittivity and thermal expansion study and the data from previous measurements [12, 10].

For a ceramic with the composition $x = 0.0$ we observed one anomaly of $\varepsilon'(T)$ at $T_c = 390$ K with classical behaviour and another very small anomaly at about 120 K with considerable frequency dispersion (figure 6(a)). The thermal expansion coefficient $\alpha(T)$ shows a well pronounced anomaly at about 390 K, a noticeable feature at ∼250 K and a pronounced change in the slope below 200 K (figure 6(b)).

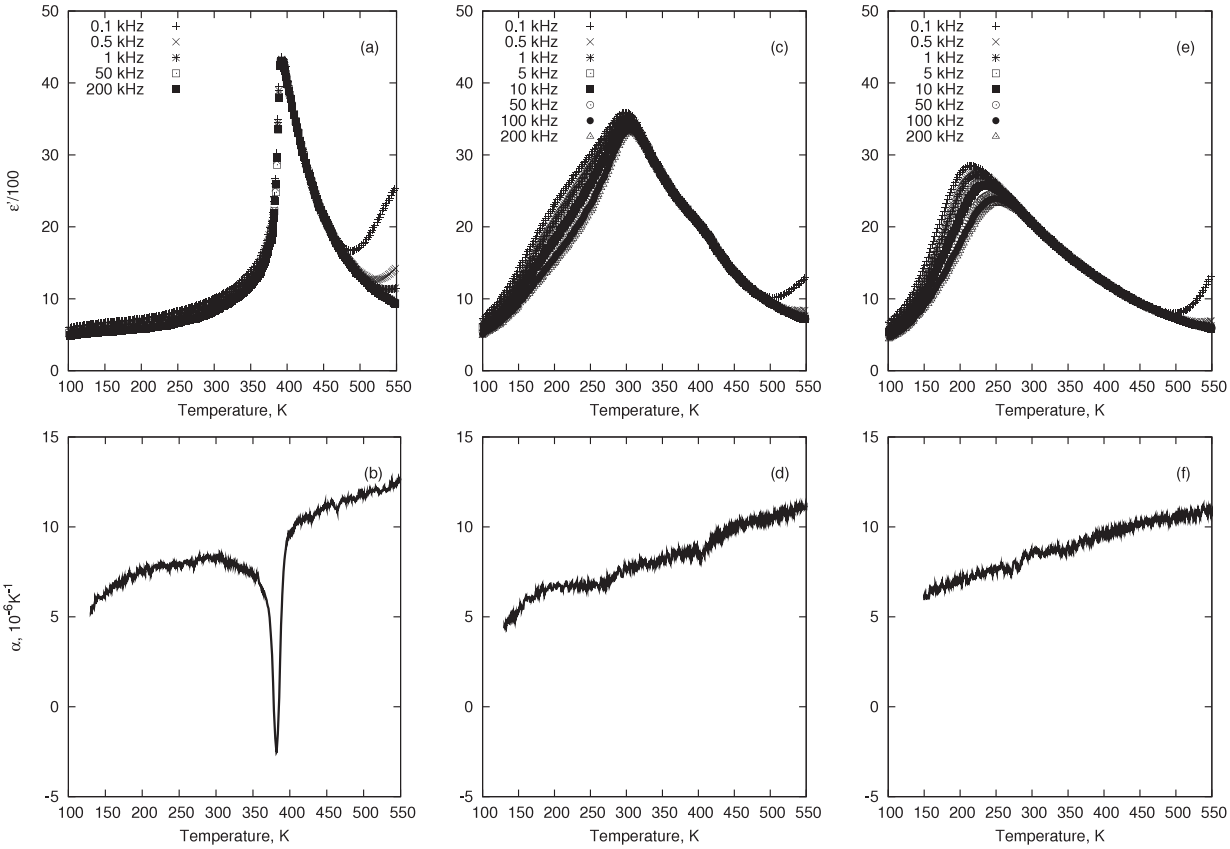

Figure 6. Temperature dependence of the real part of the permittivity ε' ((a), (c), (e)), and the thermal expansion coefficient α ((b), (d), (f)) for ceramics with composition $Ba_{0.90}Bi_{0.067}Ti_{1-x}Zr_xO_3$: (a), (b) $x = 0.0$; (c), (d) $x = 0.05$; (e), (f) $x = 0.1$.

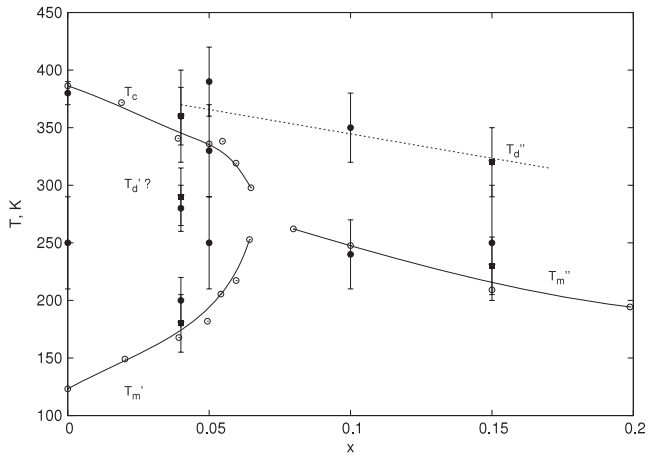

Figure 7. T–x phase diagram of $Ba_{0.90}Bi_{0.067}Ti_{1-x}Zr_xO_3$ system: ○, dielectric data [12]; ■, heat capacity and thermal expansion data [10]; ●, present study.

The high temperature anomaly of $\alpha(T)$ coincides with the anomaly of $\varepsilon'(T)$ at T_c and corresponds to the paraelectric to ferroelectric phase transition.

In the case of the $x = 0.05$ compound there are three marked anomalies of $\alpha(T)$ at 250 K, 330 K and 400 K (figure 6(d)), which approximately coincide with the anomaly and some features of $\varepsilon'(T)$ (figure 6(c)).

The presence of an additional anomaly of the thermal expansion in the temperature region 250–300 K for small concentrations of zirconium $x = 0.0$ and 0.05 (figures 6(b) and (d)) has attracted considerable attention. Its nature is not yet clear, but we can still ascribe it to the Burns temperature T_d'.

Figure 6(e) represents the temperature dependence of ε' at various frequencies for a ceramic with composition $x = 0.10$. The temperature T_m'' of the ε' maximum was shifted to higher values at greater frequencies. A frequency dispersion took place for $T < T_m''$, the value of ε_m' decreasing when the frequency increased. The thermal expansion coefficient $\alpha(T)$ shows (figure 6(f)) two very small and smeared anomalies near T_m'' and at ∼350 K, where $1/\varepsilon'(T)$ deviates from the Curie–Weiss law. We associate the first anomaly of the thermal expansion in the temperature range 350–370 K with the formation of polar nanoregions near the Burns temperature T_d'' (approximately the temperature at which the deviation of $1/\varepsilon(T)$ from the Curie–Weiss law was observed [12]) and the second one in the range 150–250 K, which coincides with the region of anomalous behaviour of the permittivity [12], with interaction of polar nanoregions near T_m''.

The difference in the phase diagrams of two systems with Bi^{3+} and La^{3+} doping is due to the difference in the charge balance compensation mechanism. In the case of La^{3+} doping compensation occurs via an ionic mechanism with partial replacement of Ba^{2+} by La^{3+} and the creation of titanium vacancies (the chemical formula $Ba_{1-x}La_xTi_{1-x/4}\square_{x/4}O_3$) leading to significant change in ferroelectric active B-sites and variation of phase transition temperatures [14]. To

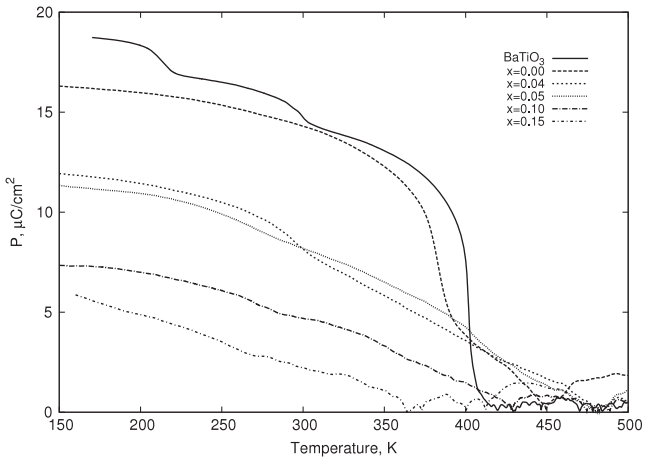

Figure 8. Root mean square polarization of $BaTiO_3$ and $Ba_{0.90}Bi_{0.067}Ti_{1-x}Zr_xO_3$ compounds.

compensate the charge imbalance in the case of Bi^{3+} doping, vacancies on the A-site are introduced, leading to the formula $Ba_{1-x}\square_{x/3}Bi_{2x/3}TiO_3$ [12]. In this case the main change takes place on nonferroactive A-sites.

Bi^{3+} (or La^{3+}) ions and cation vacancies can form defect clusters. A similar situation was observed and simulated for Nb^{5+} modified $BaTiO_3$, where relaxor behaviour takes place at Nb concentrations of more than 6% [27, 28]. At high values of dopant concentration long-range ferroelectric order can be broken down by defect clustering, but local polar order is preserved within defect-free regions giving rise to the $\varepsilon(T)$ anomaly at T'_m.

According to [12] bismuth doping leads to decline of thr $C2mm$ phase and to the occurrence of unusual relaxor phenomena at T'_m inside the ferroelectric state. It is not inconceivable that similar phenomena occur in the case of La doping; however, the temperature interval between phase transitions is small enough and it is difficult to locate T_1, T_2 and T'_m due to essential degradation and overlapping of anomalies for samples with $y \geqslant 0.036$. Nevertheless, according to [14], already at an La concentration of 0.04 and temperatures $T < T_c$ appreciable dispersion and relaxor phenomena are observed, which accrue as the concentration increases. The relaxor phenomena in compounds with heterovalent replacement of barium, in particular by La, are connected with defect cluster formation and the occurrence of the strong random electric fields destroying the homogeneous ferroelectric state [14].

Results of the $\langle P^2\rangle^{1/2}$ calculations are shown for $Ba_{0.90}Bi_{0.067}Ti_{1-x}Zr_xO_3$ and $BaTiO_3$ in figure 8.

4. Conclusions

Two systems of solid solutions $Ba_{1-y}Bi_{2y/3}Ti_{1-x}Zr_xO_3$ and $Ba_{1-y}La_yTi_{1-y/4}O_3$ have been studied by a dilatometric method. The temperature behaviour of the root mean square polarization of the solid solutions studied is compared with the data for pure $BaTiO_3$.

Both the amplitude of polarization and its variation versus temperature are in agreement with the previous dielectric data for the studied solid solutions. In the case of relaxor compositions the Burns temperature is always detected in thermal expansion experiments. In the case of Zr substitution to the Ti site, it appears that the Burns temperature is always near 400 K, the ferroelectric transition temperature of the $BaTiO_3$ parent compound.

Acknowledgments

This work was supported by the Russian Foundation for Basic Research (project no. 07-02-00069) and the Council on Grants from the President of the Russian Federation for Support of Leading Scientific Schools (project no. NSh-1011.2008.2).

References

[1] Hennings D, Schnell A and Simon G 1982 *J. Am. Ceram. Soc.* **65** 539
[2] Ravez J and Simon A 1997 *Eur. J. Solid State Inorg. Chem.* **34** 1199
[3] Farhi R, Marssi M El, Simon A and Ravez J 1999 *Eur. Phys. J.* B **9** 599
[4] Sciau Ph, Calvarin G and Ravez J 1999 *Solid State Commun.* **113** 77
[5] Ravez J and Simon A 2000 *Phys. Status Solidi* a **178** 793
[6] Ang C, Jing Z and Yu Z 2003 *J. Mater. Sci.* **38** 1057
[7] Simon A, Ravez J and Maglione M 2004 *J. Phys.: Condens. Matter* **16** 963
[8] Bokov A A, Maglione M and Ye Z-G 2007 *J. Phys.: Condens. Matter* **19** 092001
[9] Bokov A A, Maglione M, Simon A and Ye Z-G 2006 *Ferroelectrics* **337** 169
[10] Gorev M, Bondarev V, Sciau Ph and Savariault J-M 2006 *J. Phys.: Condens. Matter* **18** 4407
[11] Ravez J and Simon A 2001 *J. Solid State Chem.* **162** 260
[12] Simon A, Ravez J and Maglione M 2005 *Solid State Sci.* **7** 925
[13] Kchikech M and Maglione M 1994 *J. Phys.: Condens. Matter* **6** 10159
[14] Morrison F D, Sinclair D C and West A R 1999 *J. Appl. Phys.* **86** 6355
[15] Boulos M, Guillemet-Fritsch S, Nguyen Q, Valdez-Nava Z, Farenc J and Durand B 2008 *Silicates Industriels* at press
[16] Goldschmidt V M 1926 *Naturwissenschaften* **14** 477
[17] Mueller V, Jager L, Beige H, Abicht H-P and Muller T 2004 *Solid State Commun.* **129** 757
[18] He Y 2004 *Thermochim. Acta* **419** 135
[19] Merz W J 1949 *Phys. Rev.* **76** 1221
[20] Strukov B A, Davitadze S T, Kravchuk S N, Taraskin S A, Goltzman M, Lemanov V V and Shulman S G 2003 *J. Phys.: Condens. Matter* **15** 4331
[21] Smolenskii G A, Bokov V A, Isupov V A, Krainik N N, Pasynkov R E and Sokolov A I 1984 *Ferroelectrics and Related Materials* (New York: Gordon and Breach)
[22] Nomura S and Uchino K 1982 *Ferroelectrics* **41** 117
[23] Burns G and Dacol F H 1983 *Phys. Rev.* B **28** 2527
[24] Bhalla A S, Guo R, Cross L E, Burns G, Dacol F H and Neurgaonkar R R 1987 *Phys. Rev.* B **36** 2030
[25] Wongsaenmai S, Yimnirun R, Ananta S, Guo R and Bhalla A S 2008 *Mater. Lett.* **62** 352
[26] Lawless W N 1978 *Phys. Rev.* B **17** 1458
[27] Simon A and Ravez J 2003 *Solid State Sci.* **5** 1459
[28] Zhang R, Li J F and Viehland D 2004 *Comput. Mater. Sci.* **29** 67